Title: Hill numbers at the edge of a pandemic: rapid SARS-COV2 surveillance using clinical, pooled, or wastewater sequence as a sensor for population change

Authors: Apurva Narechania,[1,2*] Dean Bobo,[1,3] Kevin Deitz,[1] Rob Desalle,[1] Paul Planet,[1,4,5*] Barun Mathema[6*]

Affiliations:
[1]Institute for Comparative Genomics, American Museum of Natural History, New York, NY, USA
[2]Section for Hologenomics, The Globe Institute, University of Copenhagen, Copenhagen, Denmark
[3]Department of Ecology, Evolution, and Environmental Biology, Columbia University, New York, NY, USA
[4]Division of Pediatric Infectious Diseases, Children's Hospital of Philadelphia, Philadelphia, PA, USA.
[5]Department of Pediatrics, Perelman College of Medicine, University of Pennsylvania, Philadelphia, PA, USA
[6]Department of Epidemiology, Mailman School of Public Health, Columbia University, New York, NY, USA

Corresponding authors: anarechania@amnh.org; bm2055@cumc.columbia.edu; planetp@chop.edu

Keywords: Hill numbers; Information Theory; SARS-COV2; Pangenomes; Population Sweeps; Genomic Surveillance; minhash

Abstract: The COVID-19 pandemic has highlighted the critical role of genomic surveillance for guiding policy and control strategies. Timeliness is key, but rapid deployment of existing surveillance is difficult because most approaches are based on sequence alignment and phylogeny. Millions of SARS-CoV-2 genomes have been assembled, the largest collection of sequence data in history. Phylogenetic methods are ill equipped to handle this sheer scale. We introduce a pan-genomic measure that examines the information diversity of a k-mer library drawn from a country's complete set of clinical, pooled, or wastewater sequence. Quantifying diversity is central to ecology. Studies that measure the diversity of various environments increasingly use the concept of Hill numbers, or the effective number of species in a sample, to provide a simple metric for comparing species diversity across environments. The more diverse the sample, the higher the Hill number. We adopt this ecological approach and consider each k-mer an individual and each genome a transect in the pan-genome of the species. Applying Hill numbers in this way allows us to summarize the temporal trajectory of pandemic variants by collapsing each day's assemblies into genomic equivalents. For pooled or wastewater sequence, we instead compare sets of days represented by survey sequence divorced from individual infections. We do both calculations quickly, without alignment or trees, using modern genome sketching techniques to accommodate millions of genomes or terabases of raw sequence in one condensed view of pandemic dynamics. Using data from the UK, USA, and South Africa, we trace the ascendance of new variants of concern as they emerge in local populations months before these variants are named and added to phylogenetic databases. Using data from San Diego wastewater, we monitor these same population changes from raw, unassembled sequence. This history of emerging variants senses all available data as it is sequenced, intimating variant sweeps to dominance or declines to extinction at the leading edge of the COVID19 pandemic.

The surveillance technique we introduce in a SARS-CoV-2 context here can operate on genomic data generated over any pandemic time course and is organism agnostic.

One-Sentence Summary: We implement pathogen surveillance from sequence streams in real-time, requiring neither references or phylogenetics.

Main Text: The COVID-19 pandemic has been fueled by the repeated emergence of SARS-CoV-2 variants, a few of which have propelled worldwide, asynchronous waves of infection(1). First arising in late 2019 in Wuhan, China, the spread of the D614G mutation led to sequential waves of Variants of Concern (VOC) about nine months later, significantly broadening the pandemic's reach and challenging concerted efforts at its control (2). Beta and Gamma variants drove regional resurgences, but Alpha, Delta and Omicron occurred globally (3)(4). The advent of each variant led to the near extinction of the population within which it arose (5). The architecture of this pandemic is therefore marked by periods of transition, tipping a population towards an emerging variant of concern followed by its near complete sweep to dominance.

At the pandemic's outset, epidemiological work was focused on transmission networks, but SARS-CoV-2's high rates of infection quickly outstripped our ability to trace it(2). When it became clear that even focused global efforts would only characterize a fraction of infections, researchers turned to phylodynamic approaches to understand SARS-CoV-2's population structure(6)(7). Genomics was at the center of this effort. Rapid sequencing and whole genome phylogeny updated in quasi real time enabled epidemic surveillance that was a few weeks to a month behind the edge of the pandemic curve(8). In a crisis of COVID-19's scale and speed,

eliminating this analysis lag can mean the difference between timely, reasonable public health response and failure to understand and anticipate the disease's next turn.

Phylodynamics is predicated on genetic variation. Without variation, phylogenetic approaches yield star trees with no evolutionary structure. The high mutation rate among pathogens, especially among RNA viruses like SARS-CoV2, ensures the accumulation of sufficient diversity to reconstruct pathogen evolutionary history even over the relatively short time scales that comprise an outbreak. But as a genomic surveillance technique, phylodynamics is costly. Tools like Nextstrain align genomes, reconstruct phylogenies, and date internal nodes using Bayesian and likelihood approaches(9). These techniques are among the most computationally expensive algorithms in bioinformatics. Intractable beyond a few thousand sequences, phylodynamic approaches must operate on population subsamples, and subsamples are subject to the vagaries of data curation. More importantly, phylodynamic approaches are yoked to references. Most techniques are ill-equipped to respond to evolutionary novelty. We argue that genomic surveillance should herald the appearance of previously unseen variants without having to resort to comparison with assembled and curated genomes, and the lag between variant discovery and a database update is often months. Surveillance is currently hamstrung by the historical bias inherent to marker-based analysis. The existing pandemic toolbox therefore lacks unbiased approaches to quickly model the population genomics of all sequences available.

We propose a method that summarizes the temporal trajectory of pandemic variants by collapsing each day's assemblies into a single metric. In the case of pooled or wastewater sequence, this same metric is repurposed to measure survey sequence compression across days.

Our method does not subsample, perform alignments, or build trees, but still describes the major arcs of the COVID19 pandemic. Our inspiration comes from long standing definitions of diversity used in ecology. We employ Hill numbers (10)(11), extensions of Shannon's theory of information entropy(12). Rather than using these numbers to compute traditional ecological quantities like the diversity of species in an area, we use them to compute the diversity of genomic information. For example, we envision each unique k-mer a species and each genome a transect sampled from the pan-genome. Applying Hill numbers in this way allows us to measure a collection of genomes in terms of genomic equivalents, or a set of sequence pools as the effective number of sets. We show that tracing a pandemic curve with these new metrics enables the use of sequence as a real time sensor, tracking both the emergence of variants over time and the extent of their spread.

Implementation

To measure the information diversity of a population, we use ecological definitions that condense the influence of millions of genomes or terabases of raw sequence into a single value. In ecology, the effective number of species is a quantity used to provide an intuitive and simple metric for comparing species diversity across environments. Hill(10) defined the effective number of species of order q as

$$D_q = \left(\sum_i p_i^q \right)^{1/(1-q)}$$

where p_i is the frequency of a particular species i. As q tends towards one, the limit of this equation invokes Shannon's concept of generalized information entropy. The exponent of the Shannon entropy yields the effective number of species, a quantity commonly referred to as the Hill number.

$$D_1 = \exp\left(-\sum_i p_i \, ln \, p_i\right)$$

Hill numbers are best conceptualized as the number of equally abundant species required to recapitulate the measured diversity in a sample. The more diverse a sample, the higher the Hill number. The Hill number is not unique to ecological analysis. For example, in Natural Language Processing (NLP), this same quantity is termed perplexity, a key measure in the evaluation of language models(13).

While species Hill numbers are helpful for understanding the nature of any given sample, ecologists are often interested in comparisons across samples and communities. The motivation is to assess experimental design and/or to gauge the piecemeal complexity of an ecosystem. The beta diversity, a measure of differentiation between all local sites, extends species Hill numbers to Hill numbers of communities. Ecologists use the effective number of communities to understand the competing effects of their sampling and the innate diversity of their transects(14)(15)(16). The Hill number based on beta diversity is given as

$$D_\beta = \exp\left(\sum_s w_s \sum_i p_{si} \, ln \frac{p_{si}}{p_i}\right)$$

148

149 an expression that incorporates the Kullback-Leibler divergence(17) to yield the effective

150 number of communities. Here, p_{si} is the frequency of a particular species i in a particular sample

151 s, p_i is the frequency of a particular species i across all samples, and w_s weighs all observations in

152 sample s relative to all individuals censused in the experiment.

153

154 The effective number of communities measures the compressibility of the samples. If the

155 samples share many species and if individuals are evenly distributed across these species, the

156 samples essentially collapse, yielding a lower number of effective communities. If the samples

157 are highly diverse and the individuals scattered among these divergent organisms, the effective

158 number of communities approaches the number of communities sampled (Figure 1B). This

159 interpretation of the beta diversity relies heavily on information theoretic principles, reflecting

160 the broad and powerful implications of Shannon's original theory of entropy and

161 communication(12).

162

163 In the ecological framework we have described, the sample or community functions as a

164 container for observations of species and their frequencies. However, the container can be

165 anything.

166

167 Here, we reframe these equations to describe a system where the containers are either discrete,

168 clinical genomes or pools of samples. Pools can be combined at the clinic or gathered

169 downstream in wastewater. The species within these containers are enumerated strings of

170 information or k-mers. For clinical sample genomes, the effective number of communities

171 becomes the effective number of genomes, or genome equivalents. For sequences pooled by day,
172 this same quantity becomes the effective number of days. Regardless of container, we term this
173 new quantity KHILL. If we consider a set of identical sequence, KHILL will reduce to 1,
174 whereas in a set of sequence with no information overlap, KHILL will achieve its maximum, the
175 number of sets considered. The analogy is made explicit in Figure 1.
176
177 Equipped with this new metric of genome diversity, we can track population dynamics across
178 any axis of change. For clinical genomes over a defined time course, a stable community of
179 species subtypes may experience a disturbance that signifies the emergence of a new variant. If
180 selection favors this variant, the population will pass through a KHILL peak where genome
181 equivalents find a local maximum, and stable subtypes will coexist in almost equal measure with
182 the newcomer. This local maximum should erode if the new variant sweeps through the
183 population. When prior subtypes are driven to extinction and a single variant pervades, we
184 expect a local minimum for KHILL or the effective number of genomes (Figure 2A). For
185 sequence pools, we instead compare the most recent day's survey sequence to sequence from all
186 prior days. In this case, our containers are not discrete clinical genomes. Instead we calculate
187 KHILL from infection pools. These pairwise comparisons of the most recent day's k-mer pool to
188 all prior days is similar in spirit to autocorrelation, but our metric is KHILL, the information
189 diversity compressed into the effective number of days. If recent pooled sequence diverges from
190 past sequence, we expect a bend in the KHILL curve describing a change in sequence
191 compression. For pairwise comparisons, KHILL will vary between 1 and 2 (Figure 2B). We
192 mark significant changes in the time course using Bayesian Change Point detection(18).
193

194 A further application of this approach is to pangenomes, the accrued genomic content of any
195 given species(19). Because the KHILL metric functions as a measure of container equivalents
196 independent of functional content, it can bring new clarity to how pangenomes change in space
197 and time. The state of the art in pangenomes is wedded to genes and/or alignments.
198 Phylogenomic methods calculate orthologs(20), and pangenome graphs fork alignments along
199 multiple, disparate paths(21). While a number of these methods have achieved significant speed
200 (22), KHILL obviates the need for phylogenetics entirely by calculating information theoretic
201 quantities on containers of k-mers. We think not in terms of genes, but in terms of unique strings
202 of information. As we accumulate information, the KHILL curve of a transitioning population
203 will exhibit information diversity of a higher steady state than the simpler population left in the
204 wake of a selective sweep (Figure 2C).
205
206 Since the KHILL approach operates on containers of unaligned strings our main computational
207 challenge is to reduce the number of string comparisons without sacrificing sensitivity. We find
208 that a string sketch(23), as implemented in programs like MASH(24), adequately reflects
209 calculations made on the whole population. We need only a fraction of available k-mers to carry
210 each container's signal. Using a bottom-k sketch (25) of hashed strings, we accelerate KHILL
211 calculations by many orders of magnitude.
212
213 Our approach is unusual in that we are not looking for evidence of specific genetic events. With
214 sketched strings of unaligned data, we sacrifice most of the products of modern bioinformatics:
215 the discovery of mapped genome variation like alleles in particular genes, indels in non-coding
216 regions, or genome-scale structural rearrangement. But we gain a fast, intuitive metric that

summarizes the contributions of both micro-variation on the mutational scale, and macro-variation such as the presence/absence of genomic elements.

Results and Discussion

The United Kingdom is a model for COVID-19 genomic surveillance(26). The COVID-19 Genomics UK (COG-UK) consortium has accumulated more genomes and more metadata than any other regional health organization. Figure 3 shows how the seven-day moving average of the 22.2 million UK cases reported as of July 15, 2022 (panel A) has spikes coincident with the emergence of the UK's three main variants of concern: Alpha, Delta and Omicron (panel B). Panels A and B rehash the accepted epidemiological approach, case counts augmented by phylogenetic annotation. Using the complete set of 2.5 million UK genomes sequenced from these reported cases, we add panel C, a single KHILL value calculated for each day. With the emergence of each variant, KHILL rises until it reaches a local maximum where sequenced genomes are evenly distributed between the old variant and the new.

Against a background of The UK's dominant variant waves, these peaks mark clear transitions in the pandemic. Notably, the stark peaks that presage the emergence of Delta and Omicron occur well before each variant's burden of cases. In May 2021, public measures like masking and travel restrictions suppressed new infections, but it is in this month that we observe the KHILL peak signaling the arrival of Delta. The changing complexity of the viral population is reflected in this curve of daily genome equivalents regardless of the volume of cases and regardless of the variant. Because the expression for the effective number of genomes is weighted, days with just tens of sequences scale with days that may have tens of thousands.

240

241 In the UK, each population transition signified by the three KHILL peaks, were harbingers of a
242 selective sweep. A peak's ascent reflects the accumulating momentum of a variant of concern,
243 while the descent suggests this new variant's primacy. Alpha swept the population in March
244 2021 (27), Delta by July 2021 (28), and Omicron by January 2022 (29). In each case, KHILL
245 settles into a local minimum of about 1.03 effective genomes highlighting the near clonality of
246 the viral population after a variant achieves dominance. Rising KHILL values within the Delta
247 and Omicron waves suggest that we also detect accruing diversity within the Delta (mixing of
248 AY.4, B.1.617.2, and AY.4.2) and Omicron (BA.1 and BA.2) lineages over time. Though
249 evidence of evolving subvariants requires a deeper sketch (Supplemental Figure 1), this within
250 wave signal tracks the information complexity of steady evolution following a selective sweep.
251

252 We performed the same type of analysis for both the United States and South African pandemics.
253 Though we see regional differences in terms of which variants were dominant at which times, in
254 every case, the KHILL curve tracks the arrival of prevailing variants. Unlike the UK, the start of
255 the US pandemic is variably complex with near simultaneous transmission events from around
256 the world (30)(31) manifesting as a noisiness in KHILL (Supplemental Figure 2). The
257 introduction of Alpha flattens this diversity. In South Africa, the Beta variant achieved a higher
258 share of infection than in either the UK or the US (32). Though sparse genomic sampling results
259 in a stochastic KHILL curve, in SA we observe clear peaks demarcating the transitions between
260 Beta/Delta and Delta/Omicron (Supplemental Figure 3).
261

262 As SARS-CoV-2 surveillance transitioned from patient genomes gathered in the clinic to pooled
263 sequence accumulated in sewage, we extended the KHILL statistic to operate on sequence
264 dissociated with individual infections. Sequence of this type is necessarily unassembled. We
265 show that since KHILL relies only on sketched strings, reads alone produce a curve that mirrors
266 the pattern we see for all assemblies. For the curve in Supplemental Figure 4, we simulated
267 250,000 reads from each genome of a random sample of 100 genomes selected daily over the
268 course of the UK pandemic.
269
270 Pooled sequence requires that we dissolve the boundaries between these discrete infections.
271 Rather than sampling individual infections, we pool a population. To model these pools, we
272 joined and shuffled simulated reads generated for each day's infections, retaining only 400,000
273 as a kind of daily signature or sensor read for the overall state of the region. The conceptual shift
274 here is in the nature of the container. From containers of discrete genomes we transition to days
275 of pooled infections. Figure 4 features three curves chosen to highlight KHILL dynamics for the
276 three global variants. In each case, we query the curve's endpoint (most recent time point)
277 against sequence surveyed from all days prior. The emergence of each variant is marked by a
278 clear, sometimes precipitous, downturn in the value of KHILL, creating at least two starkly
279 different populations: days before the variant appeared and days after. In the case of Delta and
280 Omicron, shadows of the previous variants are also clearly visible. For statistical rigor, we apply
281 Bayesian Change Point analysis to tag significant transitions and note that these detected points
282 correspond to known population dynamics. Notably, posterior probability peaks within the
283 Omicron transition correspond to Omicron subvariants (Figure 4B).
284

285 Clearly, simulated sequence pools are amenable to KHILL surveillance analysis. But will the
286 technique work for real data? In principle, wastewater is an infection pool. Changes in
287 wastewater information diversity should expose new variants. In Figures 4C and D we show that
288 despite the noise inherent to wastewater data, we discern two clear transitions in the San Diego
289 pandemic (33): the rise of alpha in January of 2021, and the rise of omicron that December.
290 Because KHILL measures change in terms of k-mer representation and frequency across days, it
291 is sensitive to the technical errors and noise characteristic of metagenomic sequencing in a way
292 that marker-based analysis is not. To screen the noisiest time points, we calculated the alpha
293 diversity of k-mers sampled from each day and kept only those days within one standard
294 deviation of the mean (Supplemental Figure 5). This alpha diversity screen tightened our curve
295 significantly, but the emergence of delta, which is known to have dominated San Diego
296 infections by July 2021, remains hidden. Karthikeyan et al (33) use references to squash noise by
297 forcing alignment, but alignment limits novelty detection through comparison to the known.
298 Given comparable sequence coverage and depth across days, KHILL can eliminate the need for
299 references, quicken the pace of discovery, and capture incipient novelty likely to be lost to
300 marker-based analysis. Computing KHILL from pooled or wastewater reads realizes our
301 ambition of making streamed sequence a kind of online sensor (34) that can aggregate signal
302 directly and in real time and the very edge of a pandemic.
303
304 To illustrate how traditional methods lag in their detection of variant changes in a population, we
305 revisit the UK KHILL curve, focusing on the emergence of BA2. Figure 5A shows the curve
306 overlayed on version 1.2.101 Pangolin annotations. This version was released on January 28th,
307 2022. Prior to this release, it is already clear that a steady increase in the effective number of

genomes is underway, culminating in a peak just a few weeks later. But the 1.2.101 Pangolin annotation conflates this additional heterogeneity into a single annotation for B.1.1.529. About one month later, in panel B we see that the KHILL trace anticipated the arrival of a new Omicron subvariant, BA2. BA2 entered the lexicon too late to offer useful classification for what was clearly an emerging variant as early as January 1st, 2022. The BA2 classification seems to trail the BA2 KHILL peak by a full month and the beginning of the BA2 curve by two months. KHILL was picking up something new well before BA2 was fixed into the databases offering an immediacy that phylogenetic, reference-bound, and annotated techniques like Pangolin lack.

KHILL is sensitive and capable of monitoring shifts in the viral population despite the handful of changes that distinguish each variant. To better understand the number and type of phenomena we can detect with KHILL, we simulated blocks of change across 100 30kb genomes varying each population from one base to 500 contiguous bases across several classes of mutation including insertion, deletion, duplication, and transposition. (Supplemental Figure 6)(35). For SARS-CoV-2, blocks of 1 to 5 bases are biologically relevant. Within this scope, we see that 10 changes raises the effective number of genomes to about 1.05, a value that mirrors biological reality. As we would expect, any change that alters the population of k-mers (e.g., insertion) results in greater KHILL values than change that simply alters the existing k-mer counts (duplication, transposition). With frequent insertion or change over long block sizes, we see a KHILL that approaches the number of genomes simulated, a range that conveys the power of the KHILL metric to track both subtle and gross genomic change.

330 Our approach is fast, straightforward and ideally suited to durable but nimble real-time genome
331 surveillance. We calculate Figure 2C on all UK genomes available in 1800 CPU hours on low
332 memory cores. If we decrease the sketch rate by an order of magnitude, we can calculate the
333 same curve in just 180 CPU hours without losing signal from any of the UK's major variant
334 transitions (Supplemental Figure 1). The omicron autocorrelation curve in Figure 3A is similarly
335 fast. We calculate all 860 required KHILL values in 2 CPU hours. We can therefore easily
336 append daily KHILL points to the growing epidemiological time series. Recent studies struggle
337 to process all available genomes in heavily sampled regions(36). Curation can be a viable
338 strategy. In Supplemental Figure 7, we show that genome wide nucleotide diversity (π) of 100
339 randomly selected daily sequences over the UK pandemic mirrors the KHILL curve but distorts
340 its amplitude. But the time required to calculate alignments for π makes this an impractical
341 solution at the scales we've proposed here.
342
343 Though we prescribe no thresholds for marking the emergence of a new variant, our technique
344 affords public health institutions the opportunity to create actionable policy based on a simple,
345 quantitative measure. Moreover, we show that the first derivative of the KHILL curve tracks new
346 variants as deviations from a critical point, providing another potential metric to trigger policy
347 changes. During a KHILL upswing, the increasingly complex population is marked by an
348 accelerating slope, which then flattens and decelerates until the downswing settles into a variant
349 sweep (Supplemental Figure 8).
350
351 Finally, KHILL not only distinguishes the various states of genome populations along an axis of
352 change, but also quantifies exactly how much genome diversity emerges during a transition, and

353 how much is lost in a sweep. In other words, KHILL not only responds to a changing population,
354 but also integrates the effects of genetic distance, merging two primary properties of pan-
355 genomes. This is true of both the clinical and pooled samples.
356
357 Applied to genomes that comprise species level complexes, we believe that KHILL
358 accumulation curves can function as a new kind of comparative genomics realized without the
359 usual computational burden. For example, in Figure 6 we show that, in the UK population, as we
360 accumulate Delta and omicron genomes, we plateau at about 1.05 genome equivalents. Alpha
361 and Omicron BA1 asymptote at about 1.03. Higher Delta genome diversity agrees with
362 conclusions drawn from slower phylogenetic methods(37). We quickly capture this species level
363 trait using the differential saturation rate of a metric that, for any set of genome sequences,
364 collapses all genomic diversity into a single point.
365
366 KHILL is ideal for population genomics, but the approach is also relevant for biological
367 problems at other evolutionary scales. The comparative approach we highlight here might help
368 illuminate the species concept itself. With genomic containers, how many genome equivalents
369 should a legitimate species contain? Can a comparative genomics of KHILL accumulation
370 curves complement or even enhance traditional comparative genomic methods based in
371 phylogenies or networks? Moreover, containers of pooled sequence or shotgun metagenomes
372 could be used to understand the changing diversity of environmental samples in both time and
373 space. We show the potential in this type of analysis in the autocorrelations selected for Figure 3.
374

375 In this work, we use Hill numbers and the notion of container equivalents for genomic
376 surveillance. The response to the COVID-19 pandemic has resulted in some of the richest
377 biological datasets in history. Our technique is positioned to stream all this data. The state of the
378 art is burdened by alignment, a reliance on known references, and the lag characteristic of
379 retrospective databases. We do not stream through markers. Our goal is to signal population
380 change regardless of taxonomy. We see great value in a simple measure that conflates the
381 evolutionary nuance of phylodynamics without sacrificing a pandemic's actionable signals of
382 transition and sweep. The method we describe here can accommodate the massive genomic
383 datasets of future outbreaks regardless of organism, and perhaps signal when phylogenetics are
384 needed. KHILL is a new angle on the COVID19 pandemic, a technique that takes us closer to the
385 edge of one of the greatest health care challenges of our time.
386
387 **Figure Legends**
388 Figure 1. The KHILL metric. We adapt ecological definitions for beta diversity to calculate the
389 effective number of genomes (KHILL) in any set. We explicitly describe the analogy in terms of
390 variables in the KHILL expression (Panel A). Genomes with overlapping k-mer identities and
391 similar k-mer frequencies will tend to have a lower KHILL (Panel B).
392
393 Figure 2. KHILL cartoons. In a population genomic context, KHILL can be used to track
394 changing clinical genomic complexity over time and/or space. We expect that in a pandemic, a
395 Variant of Concern will increase the information diversity of a stable population. If this
396 transition is favored, the variant will sweep the population (Panel A). In a pooled or wastewater
397 context, KHILL can function as a measure of compression of unassembled, raw sequence across

398 days, with a drastic change revealing the potential arrival of a new variant (Panel B). Genomes
399 sampled from a transitioning population will exhibit higher KHILL than a population that has
400 settled into a dominant variant (Panel C).
401
402 Figure 3. The United Kingdom (UK) COVID-19 pandemic. We show new case burden (Panel A)
403 and gross phylogenetic classification (Panel B) for the UK pandemic since its inception. The
404 three distinct KHILL peaks signal the arrival of Alpha (November 2020), Delta (May 2021), and
405 Omicron (November 2022) well before each variant's spike in cases (Panel C).
406
407 Figure 4. SARS-CoV-2 in raw, pooled sequence. We extract three curves from an autocorrelation
408 analysis of simulated reads from the UK pandemic. The curves chosen focus on the three major
409 variant transitions: alpha, delta and omicron. In each case, the large downward swing marks
410 turnover from one type to another (Panel A). We show that these transitions are significant using
411 Bayesian Changepoint Detection (Panel B). San Diego wastewater data shows similar – albeit
412 noisier – transitions between variants. Comparison of raw sequence from a day dominated by
413 omicron to all prior days shows clear (Panel C) and significant (Panel D) separation between
414 alpha/epsilon and delta/omicron.
415
416 Figure 5. KHILL anticipates new variants. We show that in New York State clinical isolates, a
417 KHILL peak around December 2022 forecast the emergence of the new Omicron subvariant,
418 XBB. But this variant was not properly classified until two months later, well after XBB had
419 saturated the population (Panels A and B). We show that in the UK population, BA2's

classification was similarly delayed and only properly fixed into the Pangolin databases well after KHILL indicated BA2's population suffusion (Panels C and D).

Figure 6. SARS-CoV-2 comparative genomics. We randomly sampled 10,000 Alpha, Delta and Omicron genomes from the UK pandemic. As genomes are randomly accumulated, information diversity accrues. We show that Delta and Omicron converge on similar information diversity, but that Delta is more complex. Both are far more diverse than either Alpha or Omicron BA1 alone, an observation confirmed by phylogenetic methods on far fewer genomes.

References

1. Koelle K, Martin MA, Antia R, Lopman B, Dean NE. The changing epidemiology of SARS-CoV-2. Science. 2022 Mar 11;375(6585):1116–21.

2. Li R, Pei S, Chen B, Song Y, Zhang T, Yang W, et al. Substantial undocumented infection facilitates the rapid dissemination of novel coronavirus (SARS-CoV-2). Science. 2020 May;368(6490):489–93.

3. Dhar MS, Marwal R, Vs R, Ponnusamy K, Jolly B, Bhoyar RC, et al. Genomic characterization and epidemiology of an emerging SARS-CoV-2 variant in Delhi, India. Science. 2021 Nov 19;374(6570):995–9.

4. Viana R, Moyo S, Amoako DG, Tegally H, Scheepers C, Althaus CL, et al. Rapid epidemic expansion of the SARS-CoV-2 Omicron variant in southern Africa. Nature. 2022 Mar 24;603(7902):679–86.

441 5. Korber B, Fischer WM, Gnanakaran S, Yoon H, Theiler J, Abfalterer W, et al. Tracking Changes
442 in SARS-CoV-2 Spike: Evidence that D614G Increases Infectivity of the COVID-19 Virus. Cell.
443 2020 Aug;182(4):812-827.e19.

444 6. Grenfell BT, Pybus OG, Gog JR, Wood JLN, Daly JM, Mumford JA, et al. Unifying the
445 Epidemiological and Evolutionary Dynamics of Pathogens. Science. 2004 Jan
446 16;303(5656):327–32.

447 7. Volz EM, Koelle K, Bedford T. Viral Phylodynamics. Wodak S, editor. PLoS Comput Biol. 2013
448 Mar 21;9(3):e1002947.

449 8. Gardy JL, Loman NJ. Towards a genomics-informed, real-time, global pathogen surveillance
450 system. Nat Rev Genet. 2018 Jan;19(1):9–20.

451 9. Hadfield J, Megill C, Bell SM, Huddleston J, Potter B, Callender C, et al. Nextstrain: real-time
452 tracking of pathogen evolution. Kelso J, editor. Bioinformatics. 2018 Dec 1;34(23):4121–3.

453 10. Hill MO. Diversity and Evenness: A Unifying Notation and Its Consequences. Ecology. 1973
454 Mar;54(2):427–32.

455 11. Alberdi A, Gilbert MTP. A guide to the application of Hill numbers to DNA-based diversity
456 analyses. Mol Ecol Resour. 2019 Jul;19(4):804–17.

457 12. Shannon CE. A Mathematical Theory of Communication. Bell Syst Tech J. 1948
458 Jul;27(3):379–423.

459 13. Brown P, Pietra SD, Pietra VD, Lai J, Mercer R. An Estimate of an Upper Bound for the
460 Entropy of English. CL. 1992;

461 14. Jost L. PARTITIONING DIVERSITY INTO INDEPENDENT ALPHA AND BETA COMPONENTS.
462 Ecology. 2007 Oct;88(10):2427–39.

463 15. Marcon E, Hérault B, Baraloto C, Lang G. The decomposition of Shannon's entropy and a
464 confidence interval for beta diversity. Oikos. 2012 Apr;121(4):516–22.

465 16. Marcon E, Scotti I, Hérault B, Rossi V, Lang G. Generalization of the Partitioning of Shannon
466 Diversity. Thioulouse J, editor. PLoS ONE. 2014 Mar 6;9(3):e90289.

467 17. Kullback S, Leibler RA. On Information and Sufficiency. Ann Math Stat. 1951 Mar;22(1):79–
468 86.

469 18. Barry D, Hartigan JA. A Bayesian Analysis for Change Point Problems. J Am Stat Assoc. 1993
470 Mar;88(421):309.

471 19. Tettelin H, Masignani V, Cieslewicz MJ, Donati C, Medini D, Ward NL, et al. Genome
472 analysis of multiple pathogenic isolates of *Streptococcus agalactiae* : Implications for the
473 microbial "pan-genome." Proc Natl Acad Sci. 2005 Sep 27;102(39):13950–5.

474 20. Nichio BTL, Marchaukoski JN, Raittz RT. New Tools in Orthology Analysis: A Brief Review of
475 Promising Perspectives. Front Genet [Internet]. 2017 [cited 2022 May 25];8. Available
476 from: https://www.frontiersin.org/article/10.3389/fgene.2017.00165

477 21. Eizenga JM, Novak AM, Sibbesen JA, Heumos S, Ghaffaari A, Hickey G, et al. Pangenome
478 Graphs. Annu Rev Genomics Hum Genet. 2020 Aug 31;21(1):139–62.

479 22. Turakhia Y, Thornlow B, Hinrichs AS, De Maio N, Gozashti L, Lanfear R, et al. Ultrafast
480 Sample placement on Existing tRees (UShER) enables real-time phylogenetics for the SARS-
481 CoV-2 pandemic. Nat Genet. 2021 Jun;53(6):809–16.

482 23. Broder AZ. On the resemblance and containment of documents. In: Proceedings
483 Compression and Complexity of SEQUENCES 1997 (Cat No97TB100171) [Internet]. Salerno,
484 Italy: IEEE Comput. Soc; 1998 [cited 2022 May 25]. p. 21–9. Available from:
485 http://ieeexplore.ieee.org/document/666900/

486 24. Ondov BD, Treangen TJ, Melsted P, Mallonee AB, Bergman NH, Koren S, et al. Mash: fast
487 genome and metagenome distance estimation using MinHash. Genome Biol. 2016
488 Dec;17(1):132.

489 25. Cohen E. Size-Estimation Framework with Applications to Transitive Closure and
490 Reachability. J Comput Syst Sci. 1997 Dec;55(3):441–53.

491 26. The COVID-19 Genomics UK (COG-UK) consortium. An integrated national scale SARS-CoV-
492 2 genomic surveillance network. Lancet Microbe. 2020 Jul;1(3):e99–100.

493 27. Davies NG, Abbott S, Barnard RC, Jarvis CI, Kucharski AJ, Munday JD, et al. Estimated
494 transmissibility and impact of SARS-CoV-2 lineage B.1.1.7 in England. Science. 2021 Apr
495 9;372(6538):eabg3055.

496 28. Kläser K, Molteni E, Graham M, Canas LS, Österdahl MF, Antonelli M, et al. COVID-19 due
497 to the B.1.617.2 (Delta) variant compared to B.1.1.7 (Alpha) variant of SARS-CoV-2: a
498 prospective observational cohort study. Sci Rep. 2022 Dec;12(1):10904.

499 29. Paton RS, Overton CE, Ward T. The rapid replacement of the SARS-CoV-2 Delta variant by
500 Omicron (B.1.1.529) in England. Sci Transl Med. 2022 Jul 6;14(652):eabo5395.

501 30. Gonzalez-Reiche AS, Hernandez MM, Sullivan MJ, Ciferri B, Alshammary H, Obla A, et al.
502 Introductions and early spread of SARS-CoV-2 in the New York City area. Science. 2020 Jul
503 17;369(6501):297–301.

504 31. Worobey M, Pekar J, Larsen BB, Nelson MI, Hill V, Joy JB, et al. The emergence of SARS-
505 CoV-2 in Europe and North America. Science. 2020 Oct 30;370(6516):564–70.

506 32. Tegally H, Wilkinson E, Giovanetti M, Iranzadeh A, Fonseca V, Giandhari J, et al. Detection
507 of a SARS-CoV-2 variant of concern in South Africa. Nature. 2021 Apr 15;592(7854):438–
508 43.

509 33. Karthikeyan S, Levy JI, De Hoff P, Humphrey G, Birmingham A, Jepsen K, et al. Wastewater
510 sequencing reveals early cryptic SARS-CoV-2 variant transmission. Nature. 2022 Sep
511 1;609(7925):101–8.

512 34. Erlich Y. A vision for ubiquitous sequencing. Genome Res. 2015 Oct 1;25(10):1411–6.

513 35. Rice P, Longden I, Bleasby A. EMBOSS: The European Molecular Biology Open Software
514 Suite. Trends Genet. 2000 Jun;16(6):276–7.

515 36. Wilkinson E, Giovanetti M, Tegally H, San JE, Lessells R, Cuadros D, et al. A year of genomic
516 surveillance reveals how the SARS-CoV-2 pandemic unfolded in Africa. Science. 2021 Oct
517 22;374(6566):423–31.

518 37. Suratekar R, Ghosh P, Niesen MJM, Donadio G, Anand P, Soundararajan V, et al. High
519 diversity in Delta variant across countries revealed by genome-wide analysis of SARS-CoV-
520 2 beyond the Spike protein. Mol Syst Biol [Internet]. 2022 Feb [cited 2022 May 25];18(2).
521 Available from: https://onlinelibrary.wiley.com/doi/10.15252/msb.202110673

522

523 **Acknowledgements**: We thank Daniel Hooper for his contributions to this effort.

524 **Funding**:

525 National Institute of Allergy and Infectious Diseases of the National Institutes of Health under
526 award number R01AI151173 (BM)

527 Centers for Disease Control 75D30121C11102/000HCVL1-2021-55232 (PP)

528 Women's Committee of CHOP (PP)

529

530 **Author Contributions**:

531 Conceptualization: AN

532 Methodology: AN

533 Investigation: AN, DB, KD, RD, PP, BM

534 Visualization: DB, KD

535 Supervision: AN, PP, BM

536 Writing (original draft): AN

537 Writing (review and editing): AN, PP, BM

Competing interests: Authors declare that they have no competing interests.

Data and materials availability: All data sources are available in the main text or the supplementary materials. Code can be found here: https://github.com/narechan/khill.

Supplementary Materials

Supplemental methods

Table S1

Figures S1 to S8

Supplemental Methods

UK Clinical Genomes

Genomes and metadata were downloaded from the Covid-19 Genomics UK Consortium (COG-UK) https://www.cogconsortium.uk/. A custom R script (R version 4.1.3) was used to read the genomes and metadata into memory and sort genomes into one directory per day. We used collection dates to sort into daily directories. A total of 2,794,151 genomes were analyzed. The KHILL program was run on each directory with the following parameters: -k 19 -m 1 -n 100 -s 1e99 -p 6. To calculate daily cases, we downloaded covid cases data from Our World In Data https://ourworldindata.org/covid-cases. The csv file was loaded into R and filtered to include only data from the UK. To assign each genome to a clade, we used Pangolin for each genome, https://github.com/cov-lineages/pangolin (pangolin version 4.1.2; data version 1.12). The scorpio call output was used, and we summarized the clade assignments with the modifications shown in Table 1 below. Plots were made with R and ggplot2 (version 3.3.5)

USA Clinical Genomes

Genomes and metadata were downloaded from the Covid 19 Data portal (https://www.covid19dataportal.org/). A table of metadata for each genome were downloaded from the web interface. The search parameter was (country:"USA") AND (coverage:["95" TO "100"]). The accessions were fed into the CDP-File-Downloader (https://www.covid19dataportal.org/bulk-downloads), and genomes were downloaded and put into directories (one directory per day). A total of 1,926,292 genomes were analyzed for the USA using the same methods outlined for the UK above.

24 SA Clinical Genomes

25 Genomes were downloaded from GISAID EpiCov https://www.epicov.org/ We searched for
26 Location = "Africa / South Africa", selecting "Complete" and "Collection Date Complete". We
27 downloaded genomes directly from the web interface (selecting Download and then input for
28 "Input for the Augur pipeline"). Genomes were sorted into directories (one directory per day). A
29 total of 32,623 genomes were analyzed for South Africa using the methods outlined for the UK
30 above.

31

Supplemental Table 1: Scorpio Calls	
Scorpio Call	Modified Name
[blank]	Other
A.* and Alpha.*	Alpha
B.* and Beta.*	Other[†]
Delta.*	Delta
Epsilon.*	Other
Eta.*	Other
Gamma.*	Other
Iota.*	Other
Lambda.*	Other

Mu.*	Other
Omicron (XE-like)	Omicron
Omicron (Unassigned)	Omicron
Omicron (BA.1-like)	Omicron.BA.1
Omicron (BA.2-like)	Omicron.BA.2
Omicron (BA.3-like)	Omicron.BA.3
Omicron (BA.4-like)	Omicron.BA.4
Omicron (BA.5-like)	Omicron.BA.5
Probable.*	Other
Theta.*	Other
Zeta.*	Other

32

33 Pooled Clinical Samples Simulation

34 We generated survey sequence for each day during the UK pandemic by randomly selecting 100
35 genomes. We simulated Illumina reads from each of these 100 genomes using wgsim. These
36 reads can stand in for genomes in an analysis of clinical isolates, or they can be combined,
37 scrambled, and surveyed as representative of any one day. We simulated 1 million reads from
38 each sample but kept only 400,000 after all read libraries were joined. These 400,000 reads

39 formed the basis of pairwise KHILL calculations between each day and all days that came
40 before.
41
42 Sketch Depth Comparison
43 We tested how the sketch depth used during the KHILL calculation impacts the detection of
44 subvariants by calculating KHILL during the course of the UK SARS-CoV-2 pandemic using
45 sketch depths of 100 and 1,000. We used a generalized additive model to fit a cubic spline (lines)
46 with a kurtosis of 50 to these datasets independently in R using the package *mgcv* (https://cran.r-
47 project.org/web/packages/mgcv/index.html). We find that additional genetic diversity is captured
48 with deeper sketch rates, as evidenced by more variation in KHILL during the Delta and
49 Omicron waves (Supplemental Figure 1).
50
51 Diversity Simulations
52 We simulated mutations in populations of 29.9Kb SARS-CoV-2 genomes using the EMBOSS
53 tool *msbar* (24) and the SARS-CoV-2 reference (NCBI Reference Sequence: NC_045512.2) to
54 understand how numbers of mutations and mutation classes impact the KHill statistic. First, we
55 simulated populations of 1,000 genomes with 1bp SNP mutations. Mutations were simulated to
56 represent 1% - 50% of the genome in steps of 1% (i.e. 299 – 14,952 SNP mutations). Next, we
57 explored how variation in the bock size of mutations (1, 5, 10, 20, 50, 75, 100, 250 and 500 bp)
58 and mutation class impacted the KHILL statistic in populations of 100 genomes. For each block
59 size, we simulated mutation classes: insertion, deletion, SNP (or replacement for block mutations
60 greater than 1 bp), duplication, transposition (copy/paste), or "any", which is a random
61 combination of all mutation forementioned classes (Supplemental Figure 6).

62

63 KHILL vs. Nucleotide Diversity (π)

64 We tested how KHILL compares to an existing metric of population genetic diversity, Nei's
65 nucleotide diversity (π). First, we randomly subsampled 100 SARS-CoV-2 genomes from each
66 day of the UK pandemic and aligned these using *clustal omega* (www.clustal.org). Next, we
67 calculated genome-wide π from each subsample alignment using custom *perl* scripts. For each
68 day, we compared the KHILL measure to the subsample genome-wide π, and fit a linear model
69 to this relationship. Finally, we benchmarked the time required to align 2, 5, 10, 25, 50, 100, 250,
70 500, and 1,000 randomly subsampled SARS-CoV-2 genomes (from a single day during the UK
71 pandemic) using *clustal omega.* We did this to estimate the computational burden of aligning
72 genomes on the scale sequenced during the UK pandemic. Alignments are required to calculate
73 traditional population genetic measures such as π. It is important to note that these estimates of
74 computational time do not include the time required to: demultiplex and trim raw sequencing
75 data, align this data to a reference genome, generate the consensus sequences used in whole
76 genome alignment, or the calculation of π itself. We sought only to illustrate that when the
77 number of genomes reaches the thousands, the computational time to calculate traditional
78 population genetic measures becomes unmanageable (Supplemental Figure 7).

79

80 Slopes Analysis

81 We used the R package *mgcv* (https://cran.r-project.org/web/packages/mgcv/index.html) to fit a
82 cubic spine with a kurtosis of 50 to the UK covid pandemic KHILL data using a generalized
83 additive model. We extracted the first derivative F'(x), or slope, of the cubic spline to better
84 understand the rate of change of the spline fit to the KHILL data, and the general trend of the

underlying KHILL data during variant sweeps. Positive F'(x) values indicated a positive slope (increasing KHill), while negative F'(x) values indicated a negative slope (decreasing KHill). Rapid shifts in F'(x) mark rapid variant sweeps, especially when the population is dominated by a single variant, and then swept to extinction rapidly by a genetically distant variant (e.g. Delta to Omicron.BA.1 sweep) (Supplemental Figure 8). Sweeps between genetically similar subvariants (e.g. Omicron.BA.1 to Omicron.BA.2) produce more modest fluctuations in F'(x).

Supplemental Figures Legends

Supplemental Figure 1. Sketch depth and the detection of subvariants. We used a generalized additive model to fit a cubic spline (lines) with a kurtosis of 50 to the UK covid pandemic KHill statistics (y-axis, as a response to date on the x-axis), calculated with sketch rates of 100 and 1,000. Red arrows indicate the additional diversity captured with a deeper sketch during the Delta and Omicron waves.

Supplemental Figure 2. The United States (US) COVID-19 pandemic. We show new case burden (Panel A) and gross phylogenetic classification (Panel B) for the US pandemic since its inception. The arrival of Alpha (March 2021) seems to have homogenized a previously variable US viral population. The Delta surge (June 2021) moderately increases complexity, while the arrival of Omicron (December 2021) is accompanied by a KHILL spike followed by a rapid descent after Delta is forced into near extinction (Panel C).

108 Supplemental Figure 3. The South Africa (SA) COVID-19 pandemic. We show new case burden
109 (Panel A) and gross phylogenetic classification (Panel B) for the SA pandemic since its
110 inception. The arrival of both Delta and Omicron lead to KHILL spikes. Because of sparser
111 sequencing in this population, the SA data is considerably noisier than either the UK or USA.
112 Note that we also include the Beta variant here as it was a significant variant in the SA
113 pandemic.
114
115 Supplemental Figure 4. Simulated reads. We simulated 3 Mbases of Illumina sequence from
116 each of 50 randomly selected genomes taken daily over the course of the UK pandemic. We
117 show that the KHILL pandemic curve in this unassembled sequence mirrors that shown in Figure
118 2 for assembled genomes.
119
120 Supplemental Figure 5. Alpha diversity of wastewater k-mers. We plot the alpha diversity of
121 sequence gathered from each day of the San Diego wastewater sample. Because the sample is
122 amplicon based and enriched for SARS-CoV-2, higher alpha diversity indicates more unique
123 viral k-mers sequenced at a higher depth, while lower diversity is likely characteristic of over-
124 amplified, less even coverage. We remove these low complexity (and some high complexity)
125 days by taking only those samples with sequence one standard deviation from the alpha diversity
126 mean.
127
128 Supplemental Figure 6. Simulations. We simulated mutations in populations of 29.9Kb SARS-
129 CoV-2 genomes using the EMBOSS tool *msbar* (24) and the SARS-CoV-2 reference (NCBI
130 Reference Sequence: NC_045512.2) to understand how numbers of mutations and mutation

classes impact the KHILL statistic. Each population differs in the number of mutations (x-axis), mutation class (legend), and the block size of each mutation (as below). Panels A and B report the KHILL statistic (y-axis) calculated from populations of 1,000 genomes with 1bp SNP mutations. Mutations were simulated to represent 1% - 50% of the genome in steps of 1% (i.e. 299 – 14,952 mutations). Panel A reports the KHILL statistic for zero to 1,500 mutations, while the maximum number of mutations in panel B is 14,952, or 50% of the genome. Panels C and D report KHILL statistics for populations of 100 genomes and are faceted and annotated (top) by mutation block size (1, 5, 10, 20, 50, 75, and 100 bp in panel C, and 250 and 500 bp in panel D). We simulated mutation classes: insertion, deletion, SNP (or replacement for block mutations greater than 1 bp), duplication, transposition (copy/paste), or "any", which is a random combination of all mutation forementioned classes.

Supplemental Figure 7. Comparison between KHILL and genome wide nucleotide diversity (π). We show that genome wide π of 100 subsampled genomes per day across the UK pandemic, closely approximates the more data heavy KHILL curve (Panels A and B). Genome wide π is well correlated with KHILL (Panel C), but its calculation is expensive for anything beyond 100 genomes per day because of the cost incurred by whole genome alignment (Panel D).

Supplemental Figure 8. Slopes. In Panel A we used a generalized additive model to fit a cubic spline (blue line) with a kurtosis of 50 to the UK covid pandemic KHill statistics (y-axis, as a response to date on x-axis). Panel B presents the first derivative F'(x), or slope, of the cubic spline presented in Panel A. Positive values indicated a positive slope (increasing KHill), while negative values indicated a negative slope (decreasing KHill). The grey shaded area represents

the 95% confidence interval of F'(x). Panel C presents F'(x) (right y-axis) overlayed on the SARS-CoV-2 clade frequency (left y-axis) of the UK covid pandemic dataset. Alpha, Delta, and Omicron sub-variants have been collapsed (legend). In Panel B and C the horizontal dashed line at F'(x) = 0 indicates the transition point from positive to negative slopes of the fitted cubic spline.

Fig1

A

$$D_\beta = \exp\left(\sum_s w_s \sum_i p_{si}\, ln \frac{p_{si}}{p_i}\right)$$

Expression	Container	Meaning
i	Ecological	The set of all species
	Genomic	The set of all k-mers
s	Ecological	The set of all samples
	Genomic	The set of all genomes
p_{si}	Ecological	Frequency of species *i* in sample *s*
	Genomic	Frequency of k-mer *i* in genome *s*
p_i	Ecological	Frequency of species *i* across all samples
	Genomic	Frequency of k-mer *i* across all genomes (pan-genome)
w_s	Ecological	Weight of all observed individuals in sample *s*
	Genomic	Weight of all observed k-mers in sample *s*
D_β	Ecological	The effective number of samples (HILL)
	Genomic	The effective number of genomes (KHILL)

B

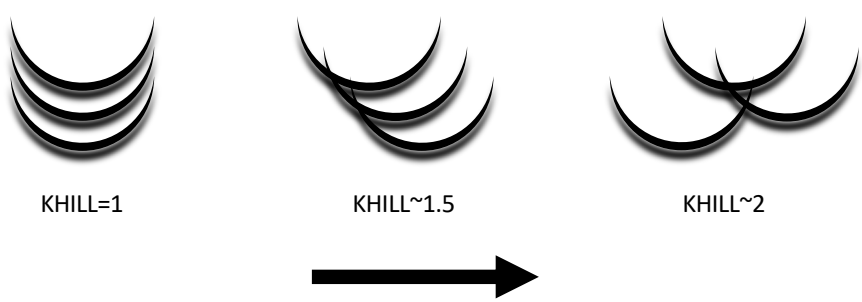

Increasing Hill number (effective number of containers)

Fig2

A

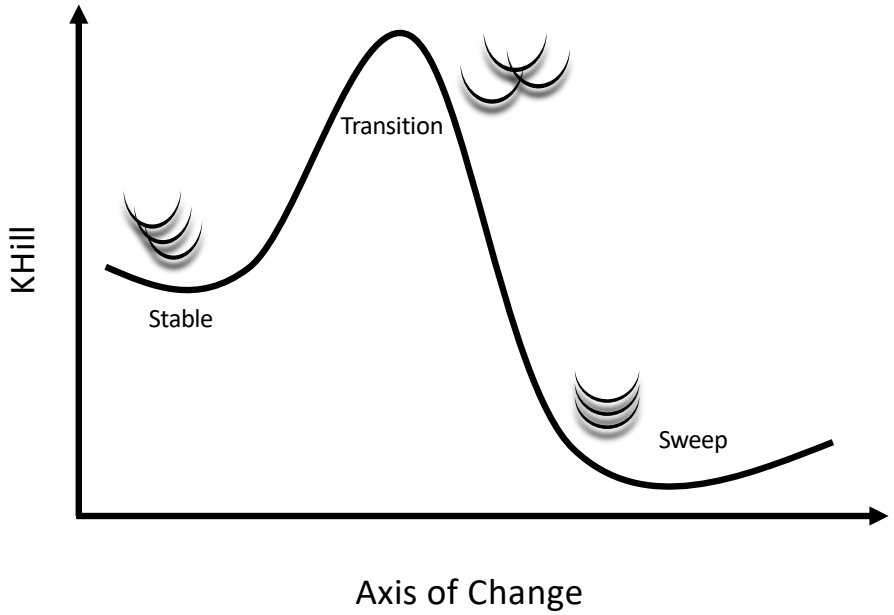

Fig2

B

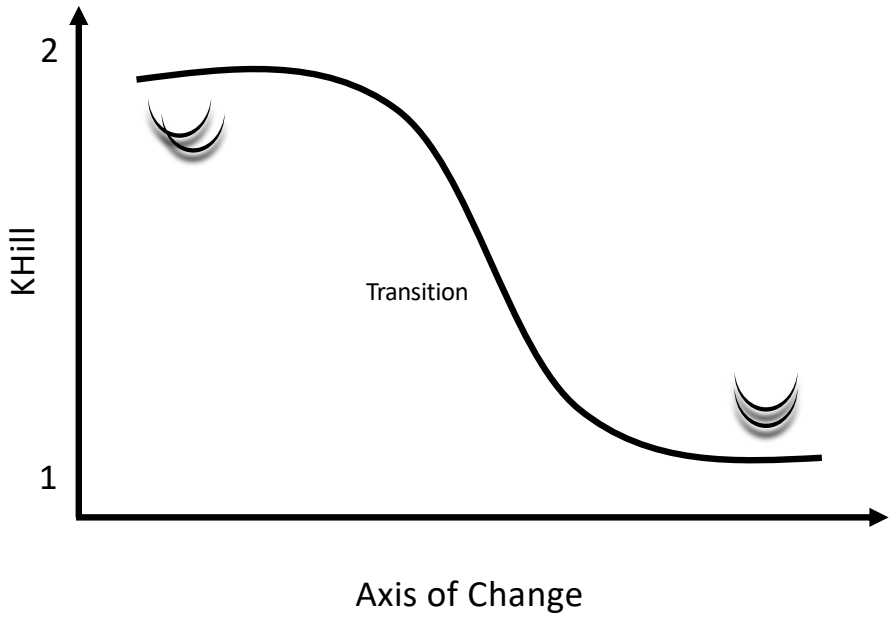
2
1
KHill
Transition
Axis of Change

C

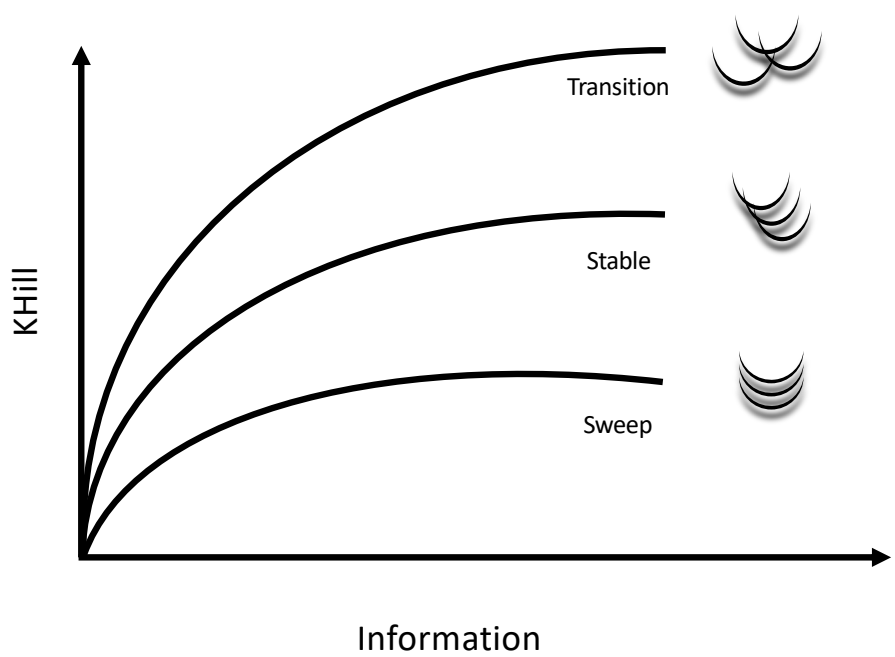
KHill
Transition
Stable
Sweep
Information

Fig3

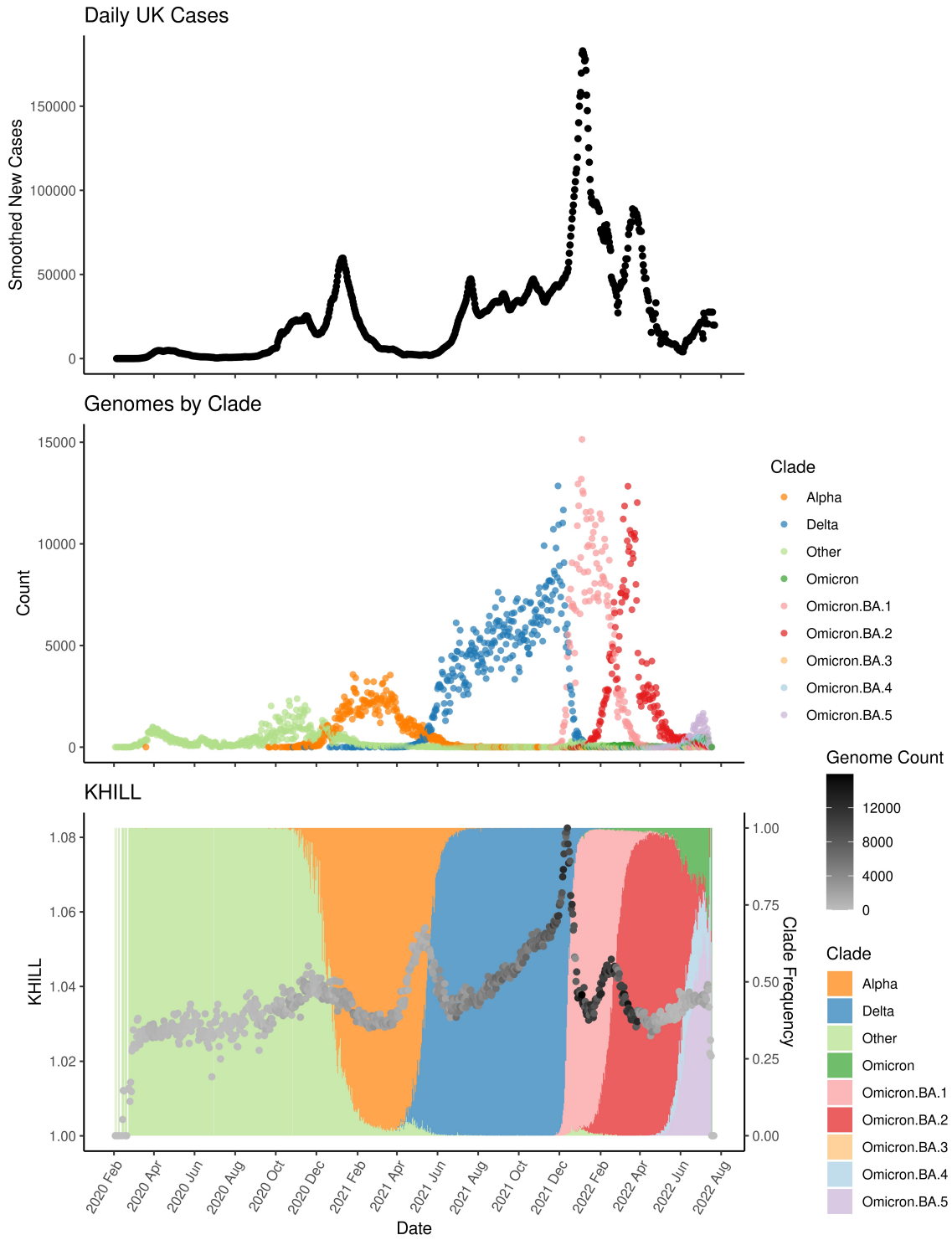
Daily UK Cases
Smoothed New Cases
150000
100000
50000
0
Genomes by Clade
Count
15000
10000
5000
0
Clade
Alpha
Delta
Other
Omicron
Omicron.BA.1
Omicron.BA.2
Omicron.BA.3
Omicron.BA.4
Omicron.BA.5
KHILL
KHILL
1.08
1.06
1.04
1.02
1.00
Clade Frequency
1.00
0.75
0.50
0.25
0.00
2020 Feb
2020 Apr
2020 Jun
2020 Aug
2020 Oct
2020 Dec
2021 Feb
2021 Apr
2021 Jun
2021 Aug
2021 Oct
2021 Dec
2022 Feb
2022 Apr
2022 Jun
2022 Aug
Date
Genome Count
12000
8000
4000
0
Clade
Alpha
Delta
Other
Omicron
Omicron.BA.1
Omicron.BA.2
Omicron.BA.3
Omicron.BA.4
Omicron.BA.5

Fig4

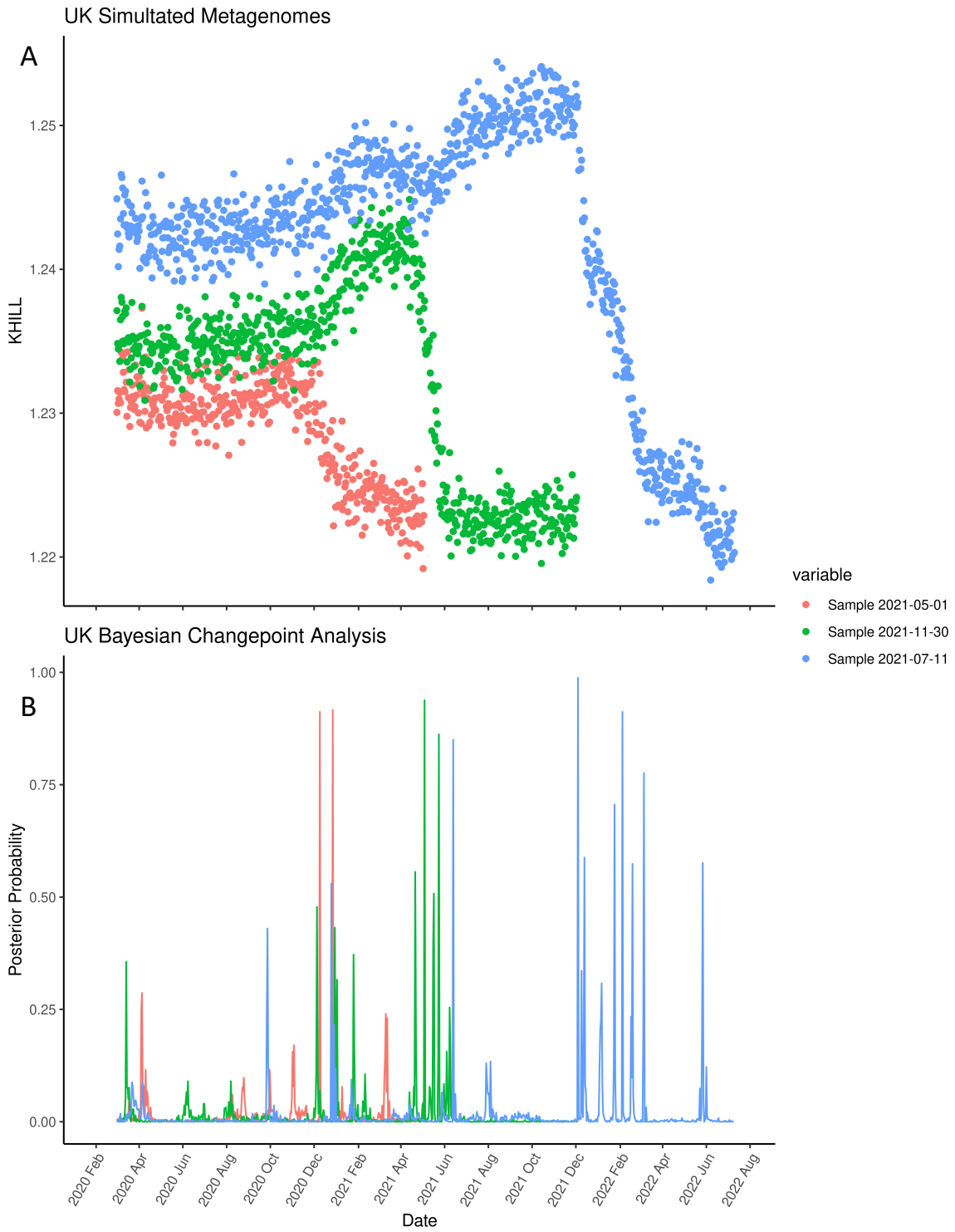
UK Simultated Metagenomes
A
KHILL
1.25
1.24
1.23
1.22
variable
Sample 2021-05-01
Sample 2021-11-30
Sample 2021-07-11
UK Bayesian Changepoint Analysis
B
Posterior Probability
1.00
0.75
0.50
0.25
0.00
2020 Feb
2020 Apr
2020 Jun
2020 Aug
2020 Oct
2020 Dec
2021 Feb
2021 Apr
2021 Jun
2021 Aug
2021 Oct
2021 Dec
2022 Feb
2022 Apr
2022 Jun
2022 Aug
Date

Fig4

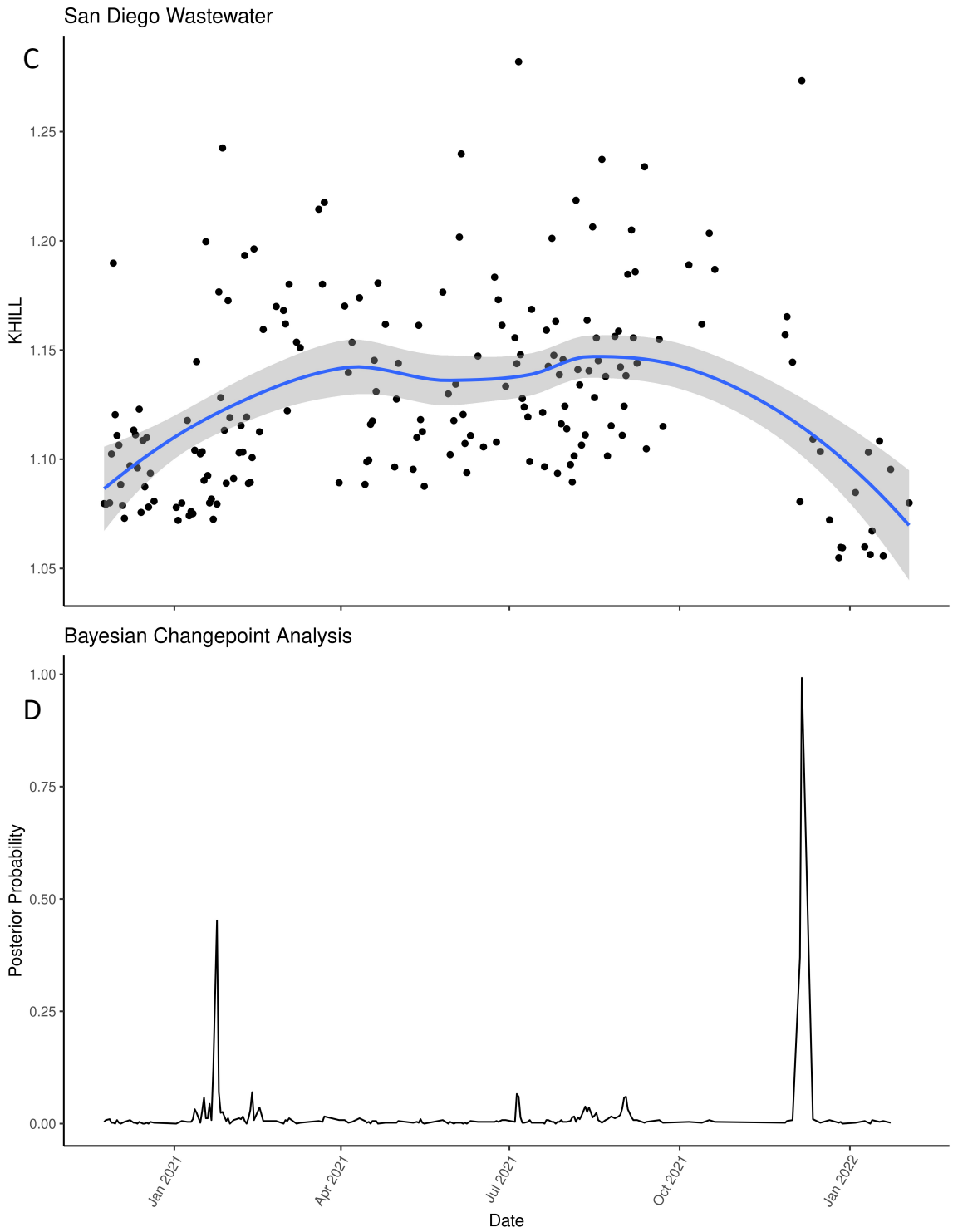
San Diego Wastewater
C
KHILL
1.25
1.20
1.15
1.10
1.05
Bayesian Changepoint Analysis
D
Posterior Probability
1.00
0.75
0.50
0.25
0.00
Jan 2021
Apr 2021
Jul 2021
Oct 2021
Jan 2022
Date

Fig5

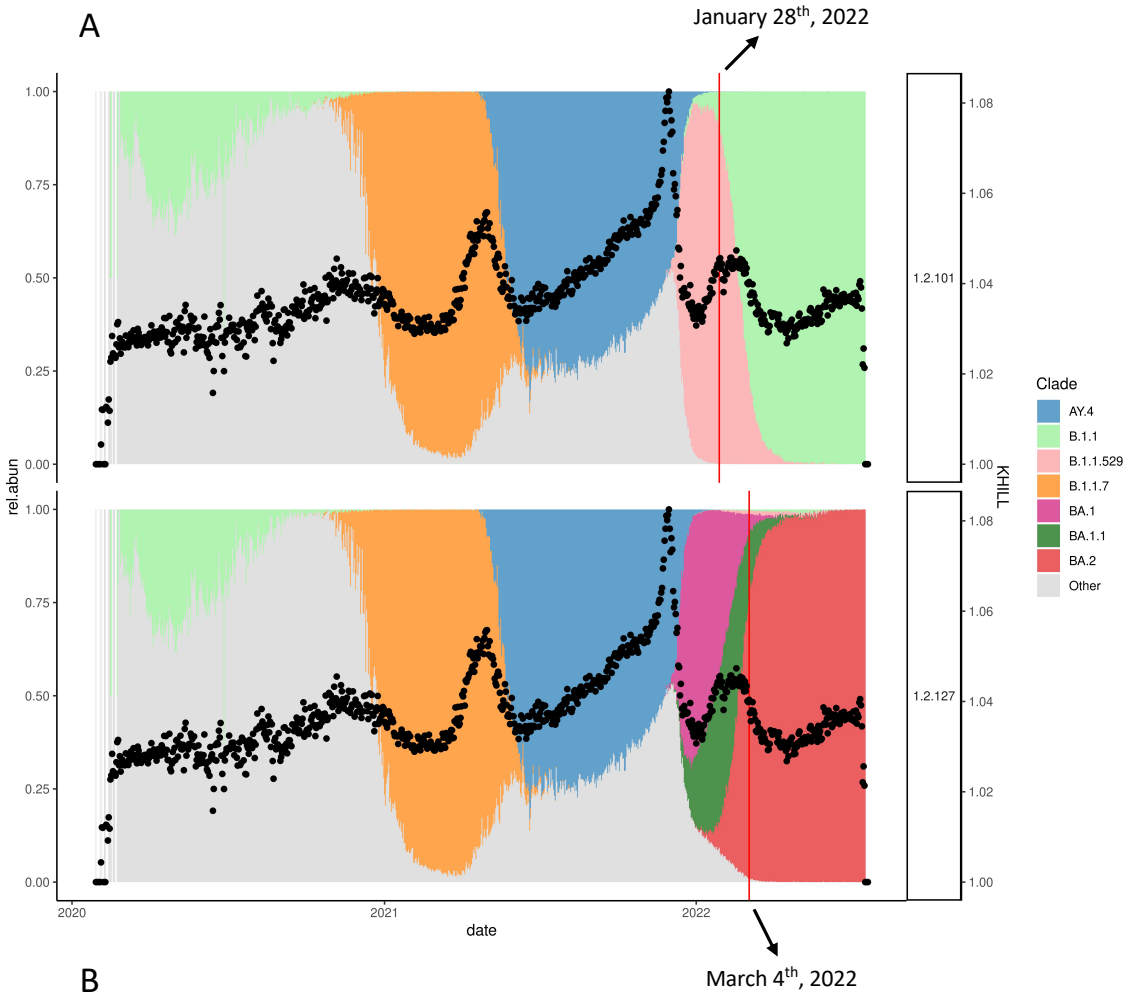
A
January 28th, 2022
1.00
0.75
0.50
0.25
0.00
rel.abun
1.2.101
1.08
1.06
1.04
1.02
1.00
KHILL
Clade
AY.4
B.1.1
B.1.1.529
B.1.1.7
BA.1
BA.1.1
BA.2
Other
1.2.127
2020
2021
2022
date
B
March 4th, 2022

Fig6

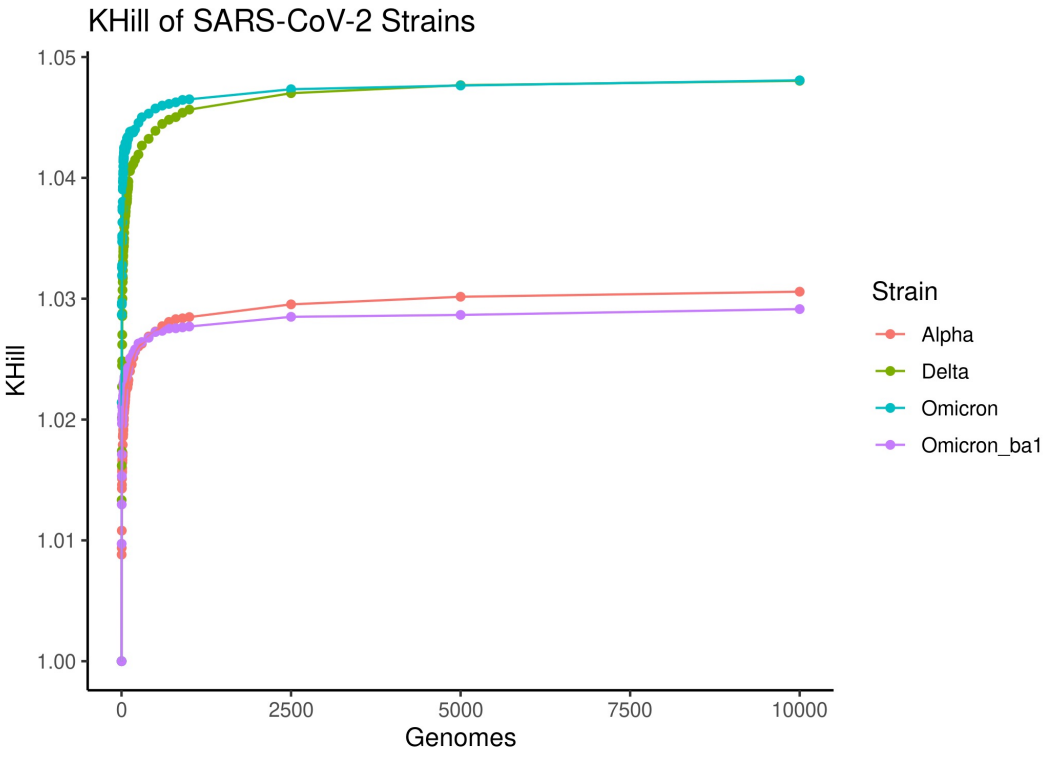
KHill of SARS-CoV-2 Strains
KHill
1.05
1.04
1.03
1.02
1.01
1.00
0
2500
5000
7500
10000
Genomes
Strain
Alpha
Delta
Omicron
Omicron_ba1

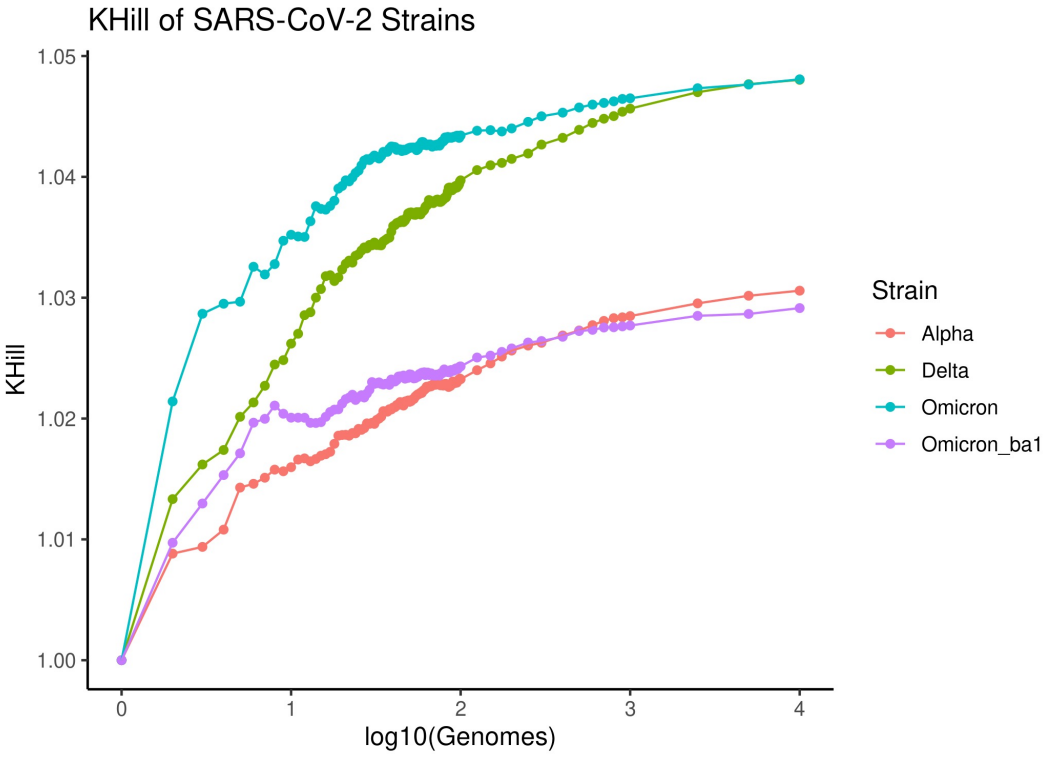
KHill of SARS-CoV-2 Strains
KHill
1.05
1.04
1.03
1.02
1.01
1.00
0
1
2
3
4
log10(Genomes)
Strain
Alpha
Delta
Omicron
Omicron_ba1

Supp Fig 1

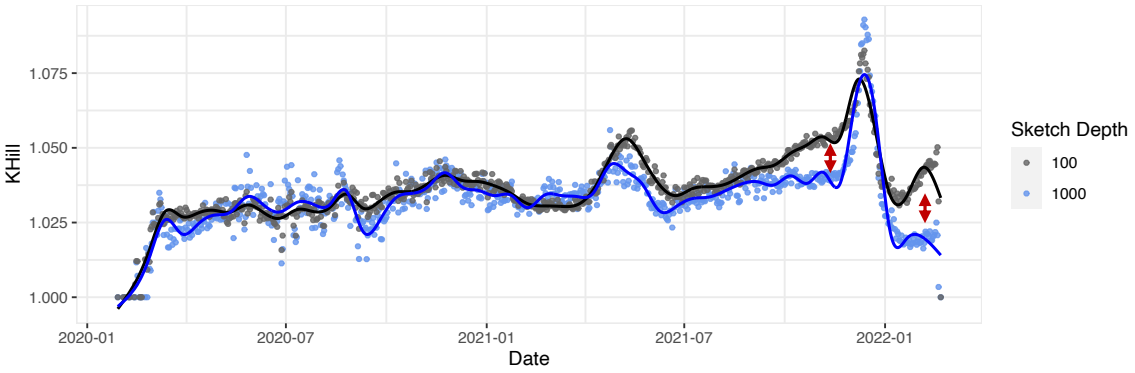
1.075
1.050
1.025
1.000
KHill
2020-01
2020-07
2021-01
2021-07
2022-01
Date
Sketch Depth
100
1000

Supp Fig 2

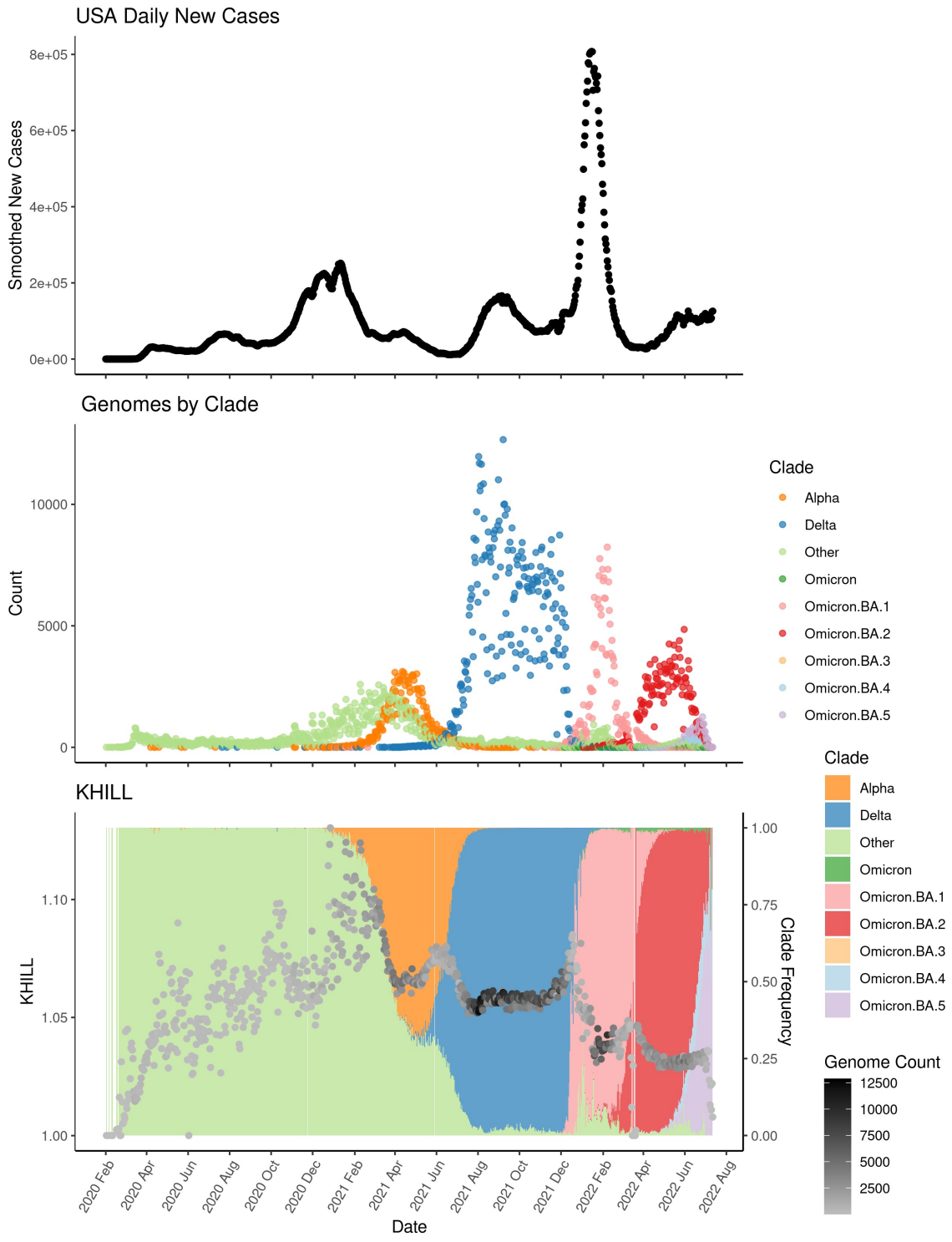
USA Daily New Cases
Smoothed New Cases
8e+05
6e+05
4e+05
2e+05
0e+00
Genomes by Clade
Count
10000
5000
0
Clade
Alpha
Delta
Other
Omicron
Omicron.BA.1
Omicron.BA.2
Omicron.BA.3
Omicron.BA.4
Omicron.BA.5
KHILL
KHILL
1.10
1.05
1.00
Clade Frequency
1.00
0.75
0.50
0.25
0.00
2020 Feb
2020 Apr
2020 Jun
2020 Aug
2020 Oct
2020 Dec
2021 Feb
2021 Apr
2021 Jun
2021 Aug
2021 Oct
2021 Dec
2022 Feb
2022 Apr
2022 Jun
2022 Aug
Date
Clade
Alpha
Delta
Other
Omicron
Omicron.BA.1
Omicron.BA.2
Omicron.BA.3
Omicron.BA.4
Omicron.BA.5
Genome Count
12500
10000
7500
5000
2500

Supp Fig 3

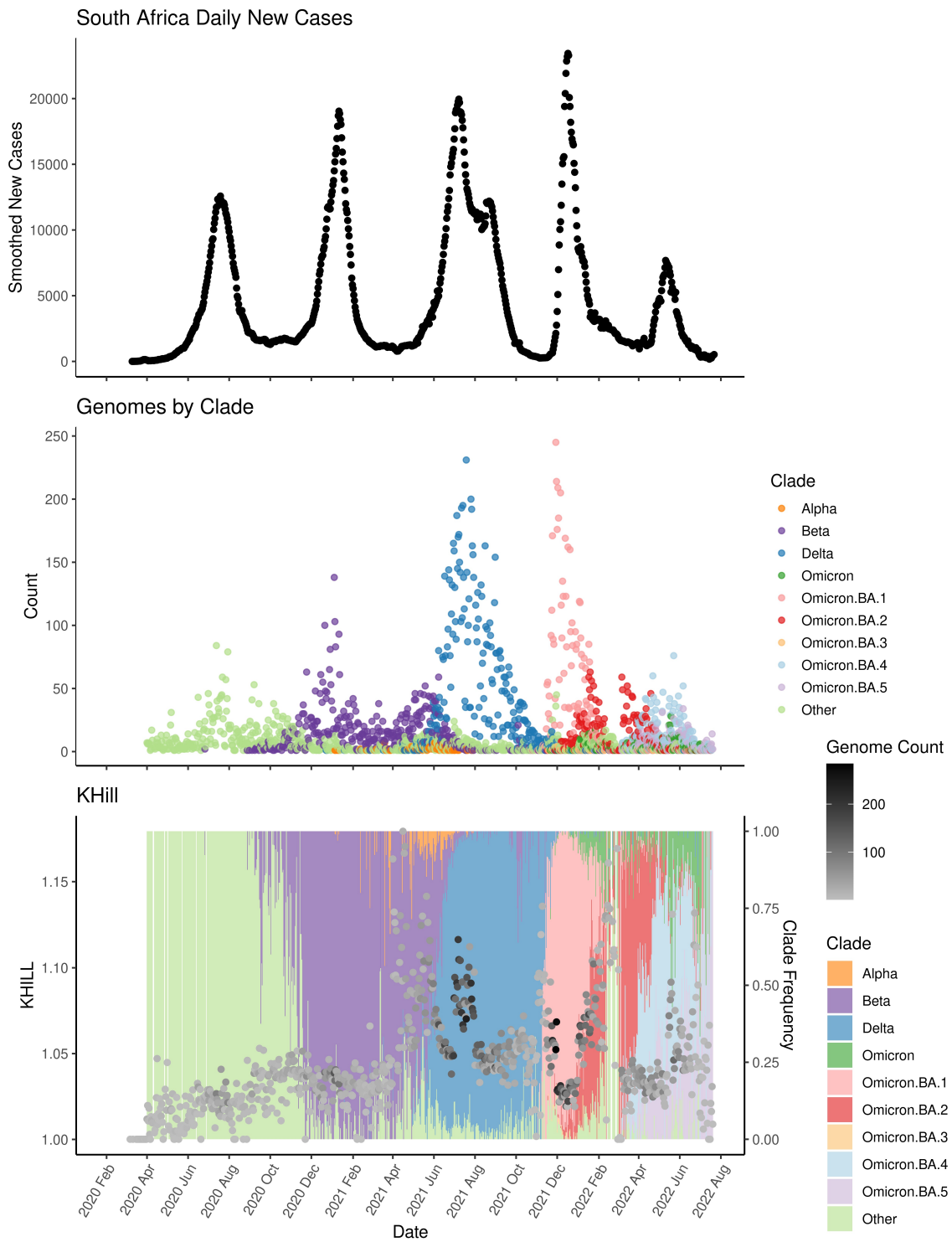
South Africa Daily New Cases
Smoothed New Cases
20000
15000
10000
5000
0
Genomes by Clade
Count
250
200
150
100
50
0
Clade
Alpha
Beta
Delta
Omicron
Omicron.BA.1
Omicron.BA.2
Omicron.BA.3
Omicron.BA.4
Omicron.BA.5
Other
Genome Count
200
100
KHill
KHILL
1.15
1.10
1.05
1.00
Clade Frequency
1.00
0.75
0.50
0.25
0.00
2020 Feb
2020 Apr
2020 Jun
2020 Aug
2020 Oct
2020 Dec
2021 Feb
2021 Apr
2021 Jun
2021 Aug
2021 Oct
2021 Dec
2022 Feb
2022 Apr
2022 Jun
2022 Aug
Date
Clade
Alpha
Beta
Delta
Omicron
Omicron.BA.1
Omicron.BA.2
Omicron.BA.3
Omicron.BA.4
Omicron.BA.5
Other

Supp Fig 4

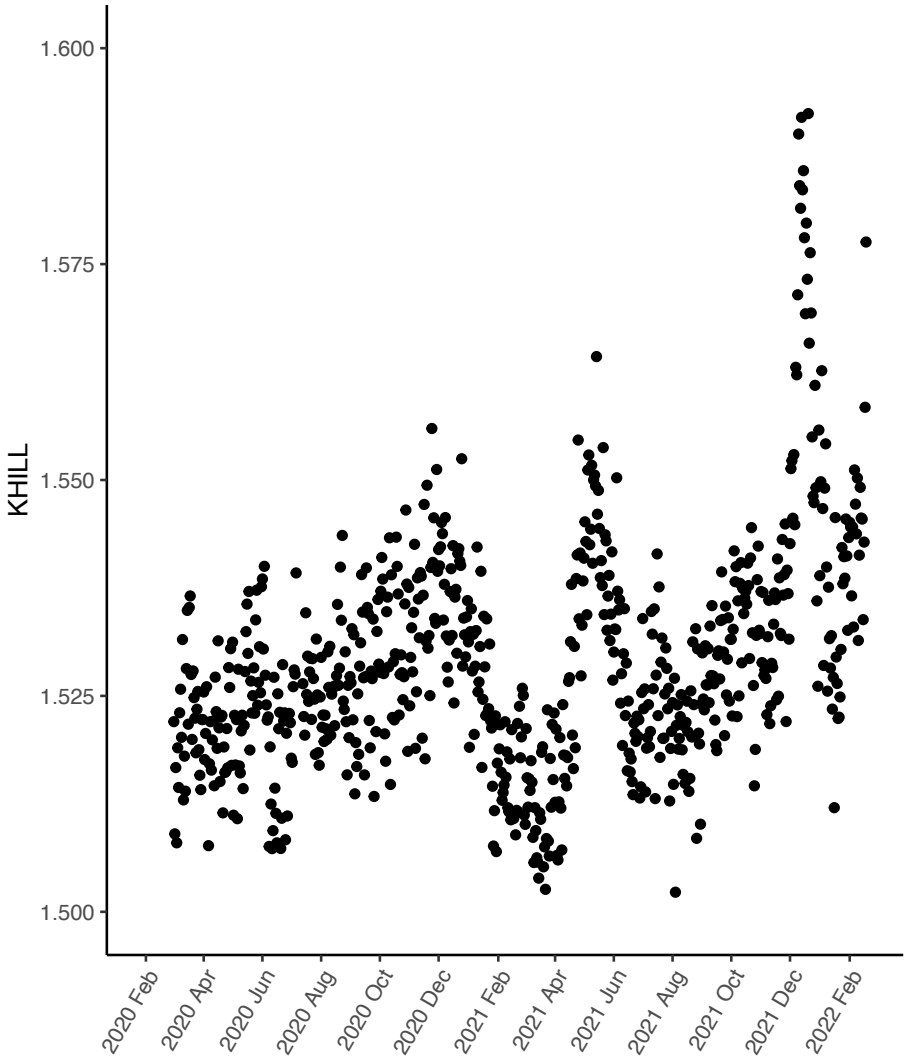
KHILL
1.600
1.575
1.550
1.525
1.500
2020 Feb
2020 Apr
2020 Jun
2020 Aug
2020 Oct
2020 Dec
2021 Feb
2021 Apr
2021 Jun
2021 Aug
2021 Oct
2021 Dec
2022 Feb

Supp Fig 5

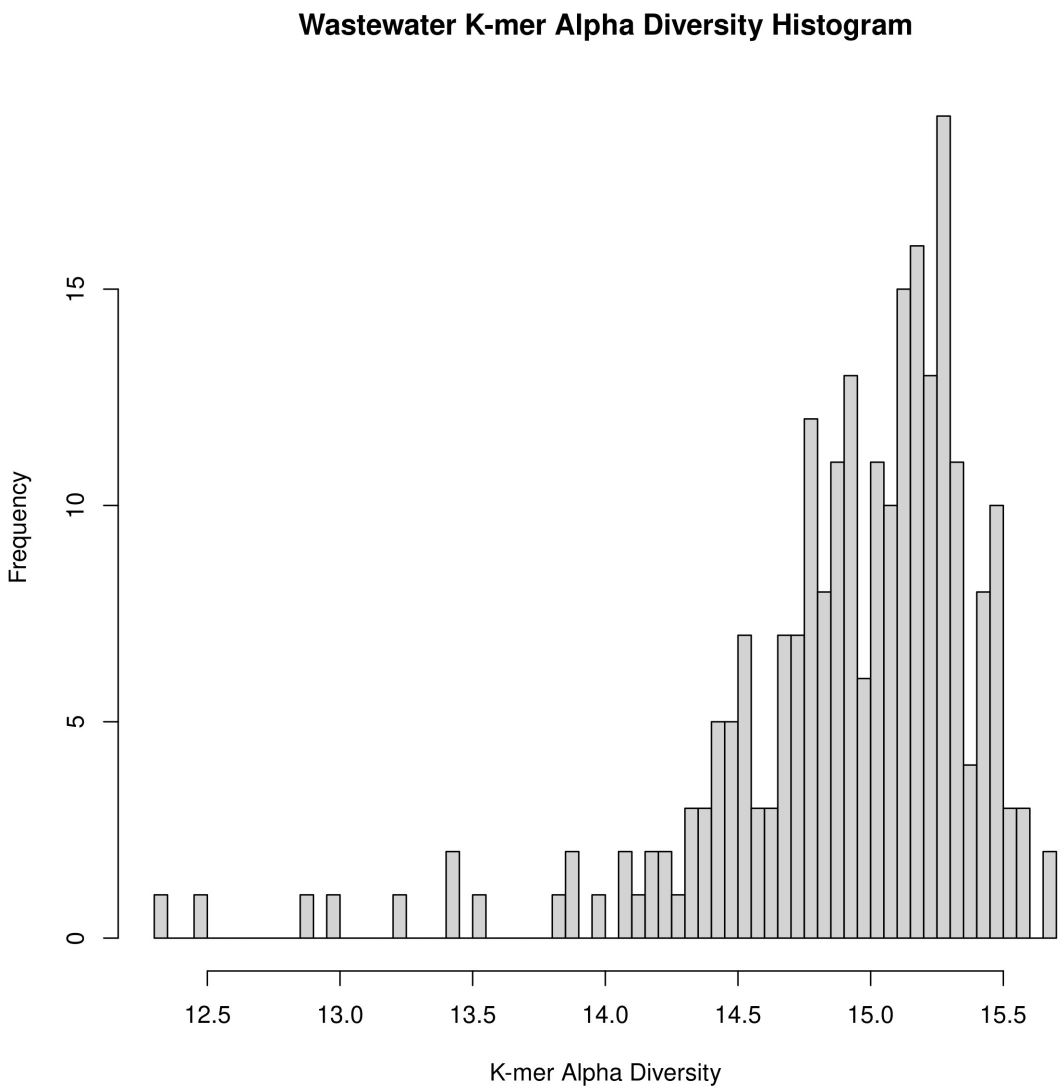
Wastewater K-mer Alpha Diversity Histogram
Frequency
0
5
10
15
12.5
13.0
13.5
14.0
14.5
15.0
15.5
K-mer Alpha Diversity

Supp Fig 6

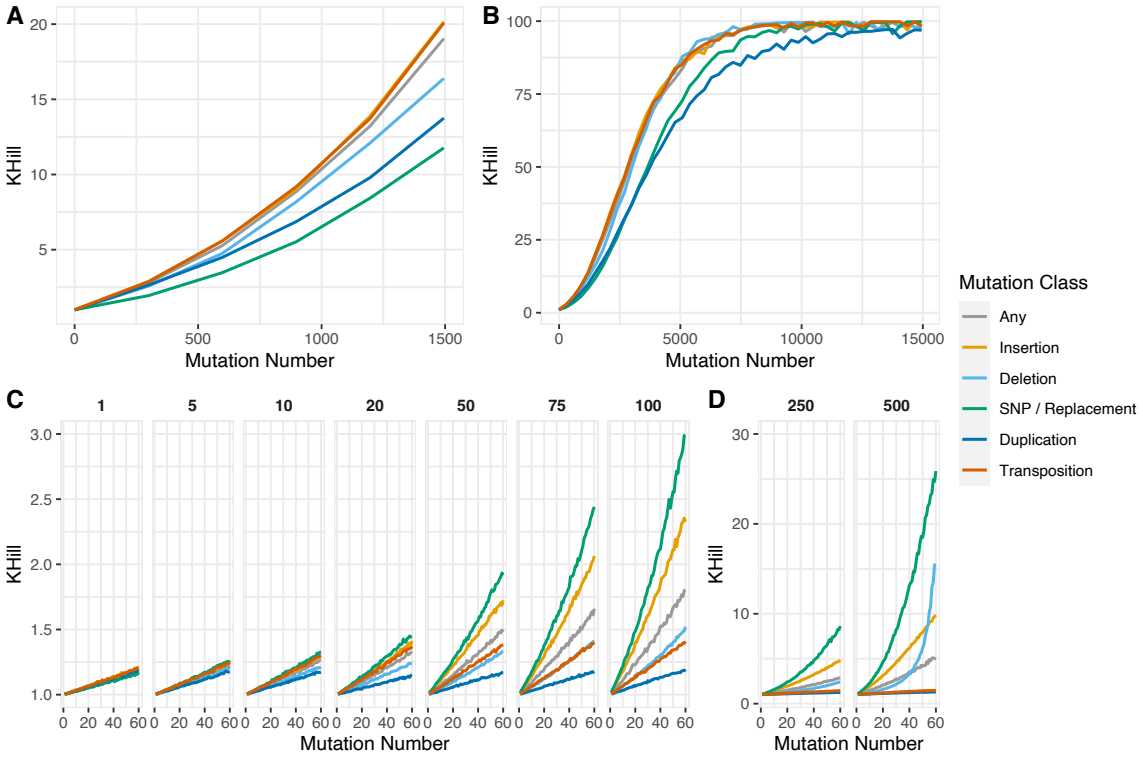
A
B
C
D
KHill
Mutation Number
1
5
10
20
50
75
100
250
500
Mutation Class
Any
Insertion
Deletion
SNP / Replacement
Duplication
Transposition

Supp Fig 7

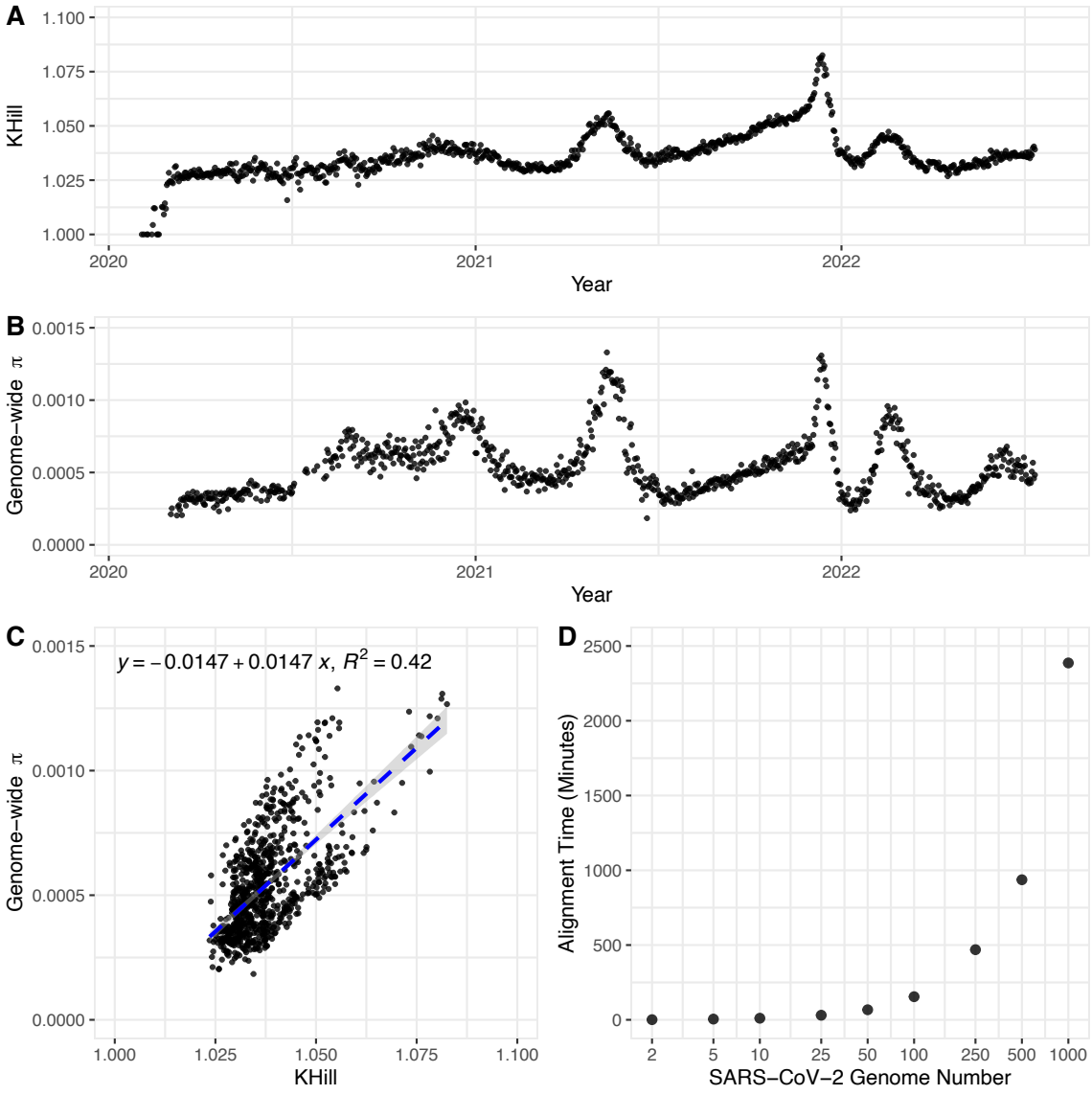
A
KHill
1.100
1.075
1.050
1.025
1.000
2020
2021
2022
Year
B
Genome−wide π
0.0015
0.0010
0.0005
0.0000
2020
2021
2022
Year
C
$y = -0.0147 + 0.0147\,x,\ R^2 = 0.42$
Genome−wide π
0.0015
0.0010
0.0005
0.0000
1.000
1.025
1.050
1.075
1.100
KHill
D
Alignment Time (Minutes)
2500
2000
1500
1000
500
0
2
5
10
25
50
100
250
500
1000
SARS−CoV−2 Genome Number

Supp Fig 8

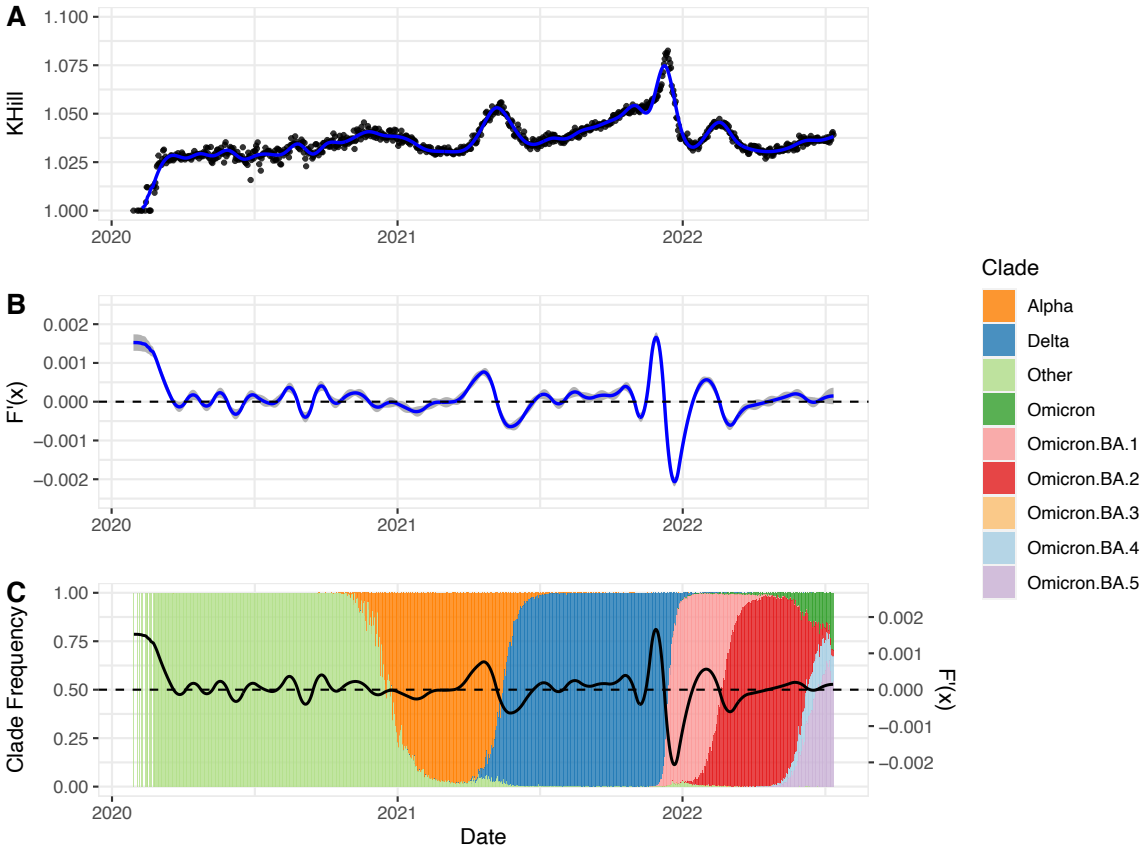
A
KHill
1.100
1.075
1.050
1.025
1.000
2020
2021
2022
B
F'(x)
0.002
0.001
0.000
−0.001
−0.002
C
Clade Frequency
1.00
0.75
0.50
0.25
0.00
F'(x)
Date
Clade
Alpha
Delta
Other
Omicron
Omicron.BA.1
Omicron.BA.2
Omicron.BA.3
Omicron.BA.4
Omicron.BA.5